LA-UR-17-27380
Approved for public release; distribution is unlimited.

Title: Maximum credibly yield for deuteriuim-filled double shell imaging targets meeting requirements for yield bin Category A

Author(s): Wilson, Douglas Carl
Loomis, Eric Nicholas

Intended for: Maximum credible yield memo for a NIF target

Issued: 2017-08-17

August 16, 2017

TO: Pat Epperson, NIF Operations

FROM: Douglas C. Wilson and Eric Loomis

SUBJECT: *Maximum credible yield for deuterium-filled double shell imaging targets meeting requirements for yield bin Category A*

I. Summary

We are anticipating our first NIF double shell shot using an aluminum ablator and a glass inner shell filled with deuterium shown in figure 1. The expected yield is between a few 10^{10} to a few 10^{11} dd neutrons. The maximum credible yield is 5e+13. This memo describes why, and what would be expected with variations on the target.

This memo evaluates the maximum credible yield for **deuterium filled double shell capsule targets with an aluminum ablator shell and a glass inner shell** in yield Category A (< 10^{14} neutrons). It also pertains to fills of gas diluted with hydrogen, helium (^{3}He or ^{4}He), or any other fuel except tritium. This memo does not apply to lower z ablator dopants, such as beryllium, as this would increase the ablation efficiency. This evaluation is for 5.75 scale hohlraum targets of either gold or uranium with helium gas fills with density between 0 and 1.6 mg/cc. It could be extended to other hohlraum sizes and shapes with slight modifications.

At present only laser pulse energies up to 1.5 MJ were considered with a single step laser pulse of arbitrary shape. Since yield decreases with laser energy for this target, the memo could be extended to higher laser energies if desired. These maximum laser parameters of pulses addressed here are near the edge of NIF's capability, and constitute the operating envelope for experiments covered by this memo. We have not considered multiple step pulses, would probably create no advantages in performance, and are not planned for double shell capsules.

The main target variables are summarized in Table 1 and explained in detail in the memo. Predicted neutron yields are based on 1D and 2D clean simulations.

	Nominal	Allowed Fielding, Category A
Drive		
Laser Energy	1.0	0-1.5 MJ
Laser Pulse	4.4ns fwhm	Any single pulse
Xray Preheat (Photons > 1.8 keV)	Nominal 2D	0 to Any
Drive Multiplier	1.0	0 to 1
Backscatter	0	0 to 100%
Hohlraum Material	Au	Au or U
Hohlraum Fill Gas Density	0.3 mg/cc	0-1.6 mg/cc
Capsule		
Ablator Material	Al	Aluminum (no dopant Z < 14)
Ablator Radius	1110 um	≤ 1200 um
Ablator Thickness	106	Any
Cushion Material	CH	CH
Cushion Density	35 mg/cc	Any
Capsule Overcoat	GDP	GDP Plastic
Overcoat Thickness	20 um	Any
Capsule Material	Glass	Glass (SiO_2)
Capsule Outer Radius	340	Any
Capsule Shell Thickness	40 um	Any
Deuterium Fill Density	10.4 mg/cc (60 atm)	Any
Maximum Credible Yield	**2.6e+12 (2D) or 1D with preheat**	**2.8e+13 (1D no preheat)**

TABLE 1. Summary of controls to ensure yield does not exceed the limit of 10^{14} neutrons (Category A) fielding conditions. These values are based on 1-D and 2-D clean Double Shell simulations driven by the equivalent of 404 TW, 1.5 MJ into a Au-wall hohlraum (see Fig. 2 for the corresponding radiation temperature and laser time history).

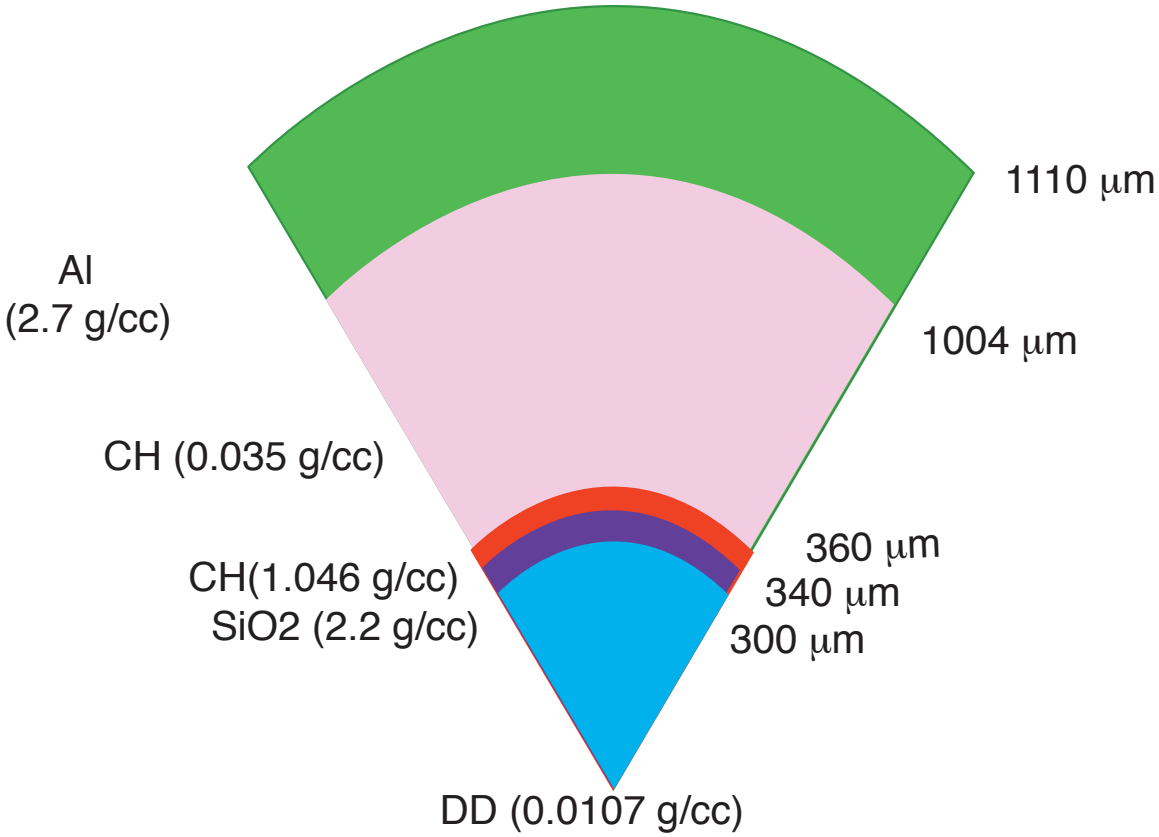

Figure 1. Nominal double shell imaging capsule.

Pulse shaping with a time dependent cone fraction is used to optimize the symmetry of a double shell implosion. Figure 2 shows the total laser power on inner cone beams (blue), outer cone beams (red) and total power (black). Since calculations in this memo are assumed to have perfect spherical symmetry, any pulse shape may be used in an experiment to achieve that symmetry. We explore only the variation of pulse width and total laser energy. We ignore the energy loss from backscatter. The nominal pulse shown in figure 2 used a time dependent cone fraction to minimize time dependent P2 and P4 asymmetry. In this memo we have varied the total energy and X-ray preheat to give 1D drives.

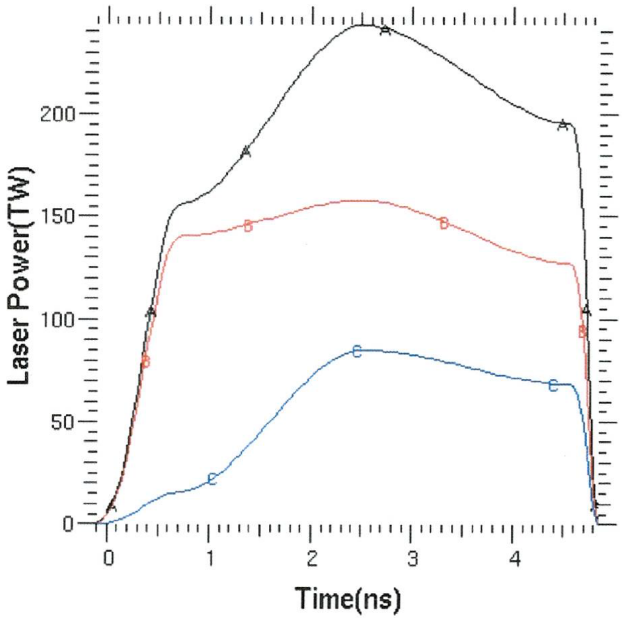

Figure 2. Nominal Laser Pulse Shape, black (A) is total power, Red (B) is power in the outer cones, Blue (C) is inner cone power. The time dependent cone fraction will be used to minimize time dependent asymmetry. The highest yields will occur with the spherical symmetry assumed in this memo.

2. Maximum Credible Yield

2.1 Simulation Methodology

Neutron yields given in this memo are from both 2D integrated and 1D radiation driven implosions. We begin with 2D simulations that include the hohlraum and laser pulse. Only in 2D simulations can parameters such as hohlraum composition (Au or U), pulse length, and pulse shape be varied in a self-consistent manner. Rather than study the effects of drive asymmetry we have artificially symmetrized the radiation field. The resulting symmetric implosion will give the highest neutron yield.

Our integrated simulations with HYDRA use Monte Carlo transport in 85 photon groups with non-LTE atomic physics. Such simulations have been shown to produce the best fidelity of output X-ray spectra, implosion symmetry, bangtimes, and yields when compared with experiments in both single shell and double shell targets. Often these require a multiplier on the laser power to match implosion times and velocities. For our current double shell capsule inside of a 5.75 mm diameter hohlraum and laser conditions, we have found that a time dependent multiplier of 0.88 gives the best match. To be conservative in this memo we have used a drive multiplier of 1.0 and assumed no backscatter, leaving the most energy to drive the capsule. Double shell experiments with 1.0 MJ have produced less than 2% SBS backscatter.

For some simulations it is impossible or undesirable to use an integrated calculation. Because the laser pulse and hohlraum spectra are coupled in an integrated calculation, it is impossible to study the effects of X-ray preheat on capsules implosions. But with a multi-frequency imposed radiation source, X-ray flux in any set of groups can be changed, and the effects of performance studied. In addition 1D calculations with an imposed radiation source are much faster, taking a few minutes, compared to several days for integrated calculations. We have extracted 1D frequency dependent sources (FDS) from our 2D calculations by tabulating the inward flux at 1.4 times the capsule radius. The 1D calculations used multi-group diffusion rather than IMC transport, and the radiation source must be specified at a boundary farther away. Deriving an FDS source that gives the same implosion hydrodynamics on a capsule as in the integrated calculation is both art and science. We found that for these capsules and an FDS source extracted from 1.4 x capsule radius, that no multiplier is needed on the overall flux, but that for photons above 1.8 keV ("M-band") a multiplier of about 2.2 is necessary. As we shall X-ray photons above 1.8 keV severely degrade capsule yield so for most of the 1D FDS driven simulations we have zeroed the radiation fluxes above 1.8 keV.

2.2 Laser Pulse

Double shell capsule performance is relatively insensitive to pulse shape variations. Part of the outer shell is ablated, and part is accelerated inward as a payload. That payload increases in velocity until it collides with and transfers kinetic energy to the inner capsule. This occurs after the end of the laser pulse, so the payload can be thought of as accumulating kinetic energy during the pulse. Variations in the pulse other than its energy have little effect on the payload kinetic energy, and on how much is transferred to the inner capsule. To demonstrate this insensitivity we have varied the nominal laser pulse in two ways. First the pulse shape itself was varied as shown in figure 3. All three pulses have the same total energy, 1.03MJ, but peak early (red) in the middle (black) and at the end of the pulse(blue).
The relatively flat pulse shown in figure 2 will be used in experiments to try to minimize laser intensity and perhaps backscatter. We have assumed no backscatter in these calculations. Figure 3 shows three variations on the laser pulse that demonstrate the relative insensitivity to laser pulse shape. The early peaking red curve gave a yield of 2.53e+12 in an integrated calculation. The nominal curve in black gave 2.61e+12, and the late peaking curve in blue gave 2.22e+12 neutrons. The nominal curve, which we used for the maximum credible yield calculations, gave the highest yield, but not by much. We conclude that changes to the shape, but not overall width, of the single laser pulse have an insignificant affect on the neutron yield.

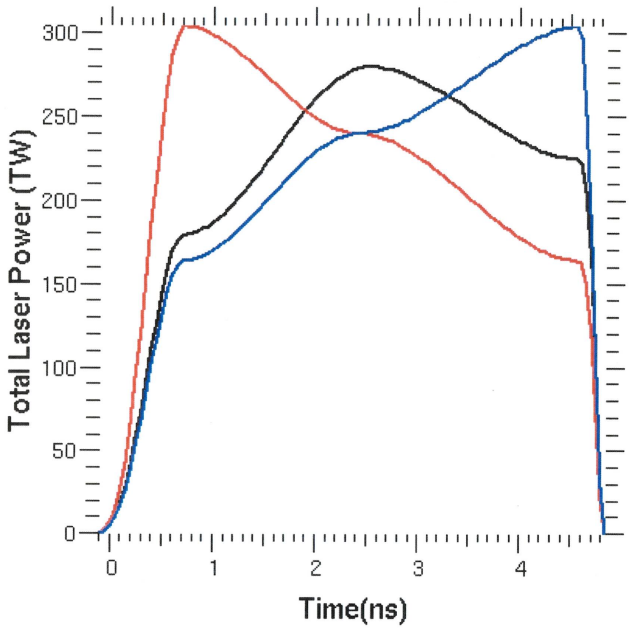

Figure 3. Variation of Pulse Shape. 1.03 MJ pulse peaking early (red), late (blue) and in the middle (black).

The shape of the single laser pulse does not produce significant yield variations under our assumptions.

A second variation of the pulse was to change its length. Figure 4 shows 6 different pulses with lengths, defined as full width at half maximum power, from 2.2 to 8.8 ns. Again the total energy is the same 1.03MJ, and both the inner and outer cone beams are scaled proportionately. The laser power was multiplied to obtain a shorter or longer pulse. All of these pulses differ from the nominal pulse, by much more than the NIF laser delivery can be expected to vary. They would have to have been specified in advance with this laser pulse. Figure 5 shows the how the neutron yield varies with pulse length. The maximum yield of 4.48e+12 is obtained at a pulse width of 5.87ns. The integrated calculation yields were: for the magenta curve, 3.11e+12; red, 2.97e+12; black 2.61e+12; green, 4.48e+12; cyan, 4.25e+12; and blue, 3.11e+12.

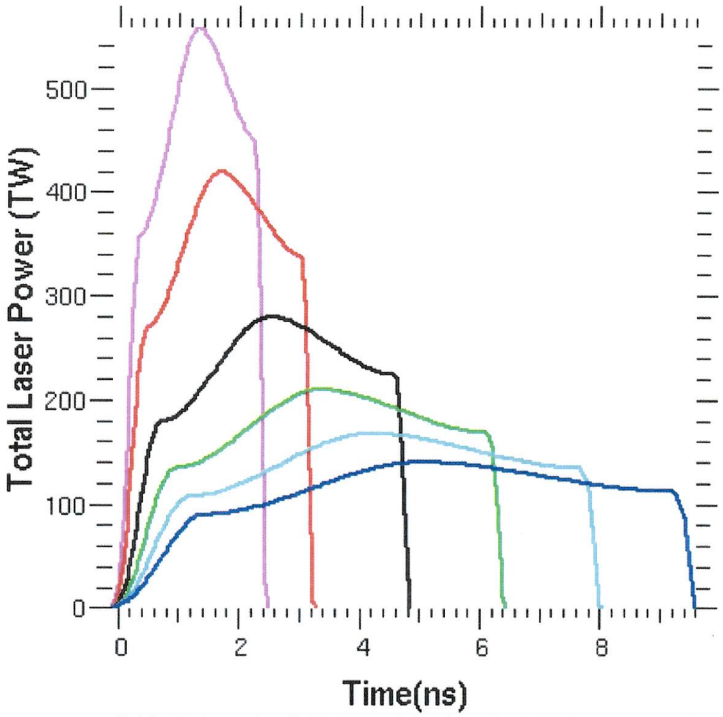

Figure 4 Laser pulses with varying widths, using the shape of the nominal pulse in both intensity and cone fraction, and 1.03MJ total laser energy.

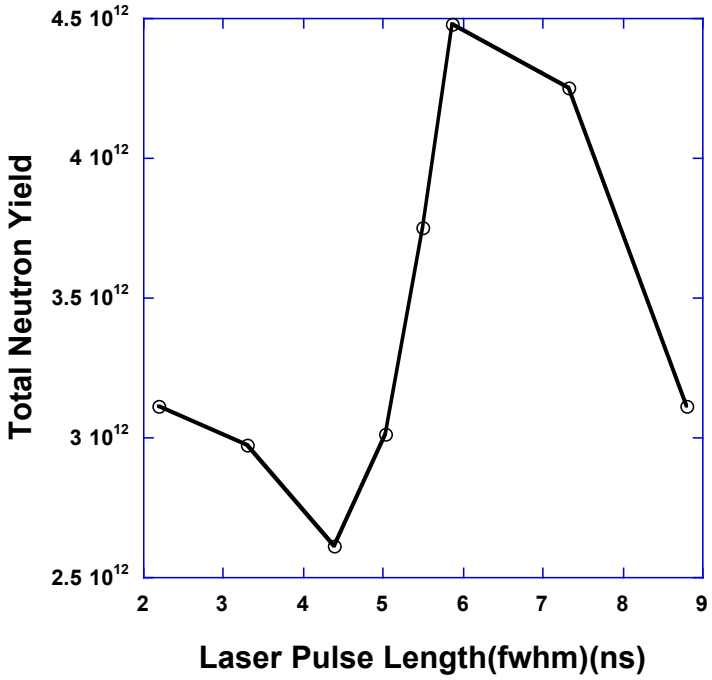

Figure 5. Variation of Total Neutron Yield in integrated calculations with the laser pulse width.

For most of the pulse width variations there is little change in the yield. But the change near 6 ns width is significant. If we want our memo to apply to all pulse

shaped, then we need to include this variation. An FDS source was extracted from the 2D integrated calculation with the 5.87ns pulse (green curve). The 1D yield from the nominal capsule with this pulse was 2.92e+13,. With the nominal pulse (black curve), it was 2.04e+13. In the following sections we will use the nominal laser pulse to explore how yield varies with target parameters. In section 3. we will include this 5.87 ns pulse as one of the possibilities in deriving a maximum credible yield. However with the optimum parameter settings from the individual parameter variations, the yield from the 5.87ns pulse drops to 2.47e+13. The maximum yield is less than 3.6e+13 we found in section 3.

2.3 Hohlraum

2.3.1 Gold vs Uranium wall

Our nominal calculation uses the 1D FDS drive from a pure gold hohlraum, as this is the only one planned for our NIF double shell experiments. However we have extracted an FDS source from a pure uranium hohlraum calculation. With uranium the peak radiation temperature rises to 273 eV from 265 as seen in figure 6. The peak drive flux is ~ 10% higher, and the preheat spectrum for photons above 1.8 keV ("M- and L-band") is shown in figure 7. The additional drive obtained by using a pure uranium hohlraum is insignificant compared to the drive variations explored later, and in fact decreases the yield. With uranium the X-ray pre-heat is slightly lower between 1.8 and 10 keV, and simply different at higher photon energies. As can be seen in both figures 7 and 8, the spectra fluxes differ, as calculated by the non-LTE atomic physics in HYDRA. Using a uranium hohlraum shifts the spectral feature to higher energy, but does not dramatically change the amount of X-ray preheat. With an uranium hohlraum the integrated capsule yield increased from 2.63 to 3.31 e+12, probably due to the preheat differences. When we applied an FDS source extracted from the uranium hohlraum calculation to the nominal capsule, the yield was 1.32e+13, less than 2.04e+13 from the same capsule in the gold hohlraum. Using the gold FDS source will lead to higher maximum credible yields. Since we eliminated preheat in our nominal calculations, and considered much larger drive flux changes, the different U pre-heat does not affect our conclusions.

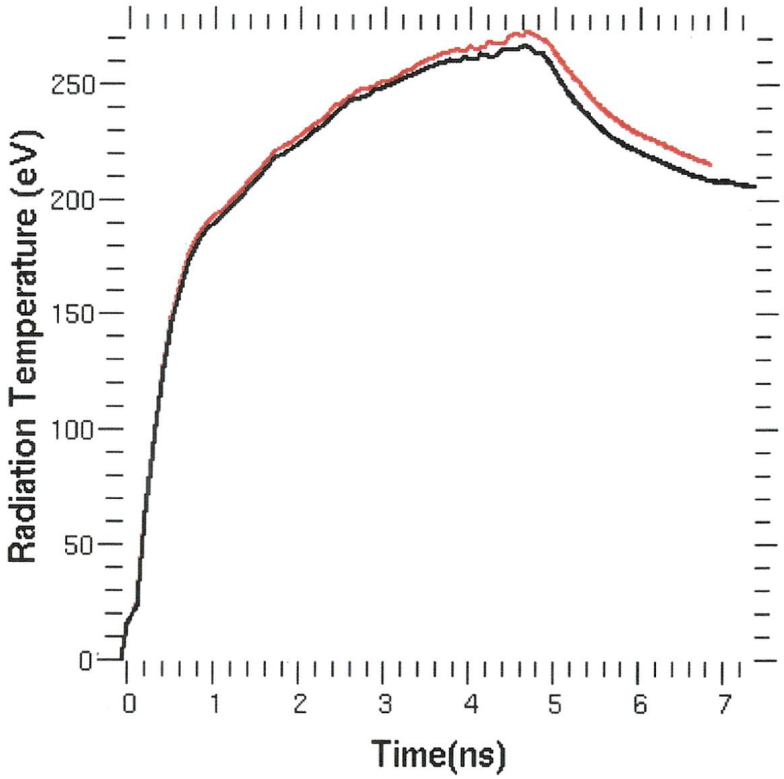

Figure 6. Time dependent radiation temperature in both gold (black) and uranium (red) hohlraums from integrated calculations.

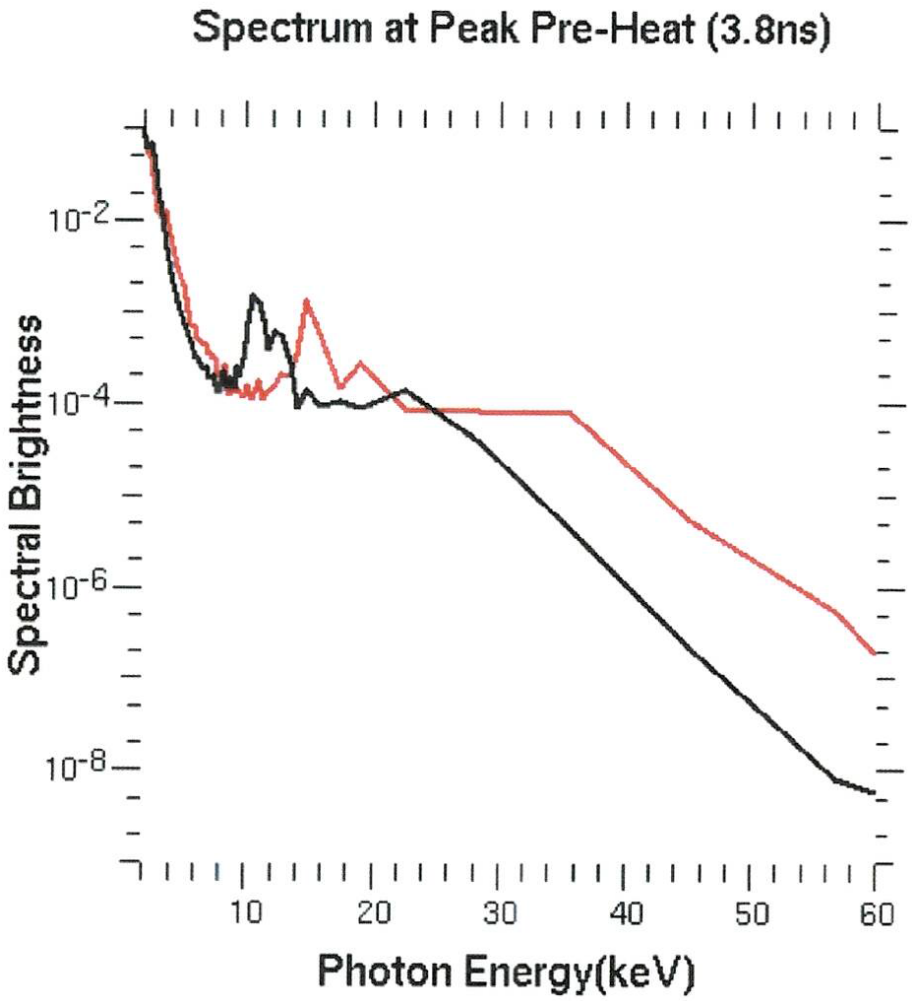

Figure 7. X-ray spectrum above 1.8 keV from both uranium (red) and gold (black) hohlraums.

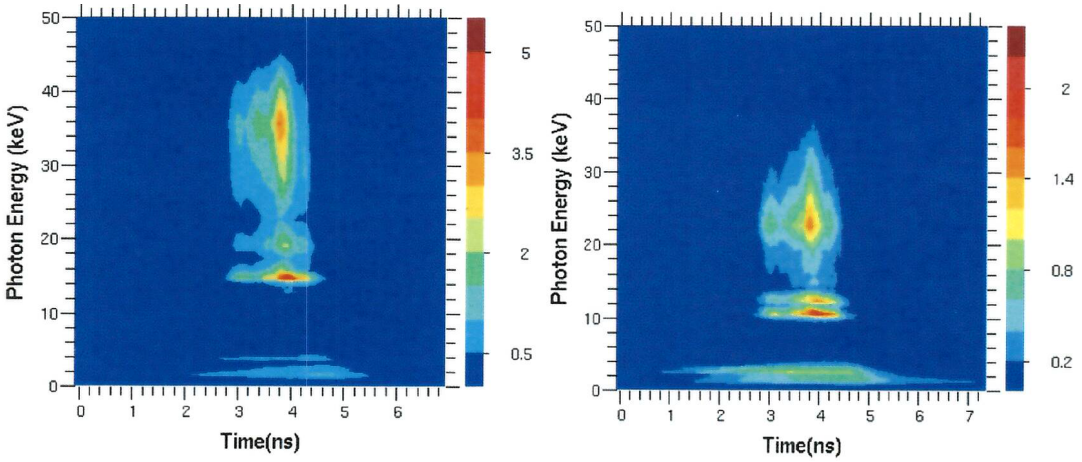

Figure 8. Time dependent X-ray spectra above 1.8 keV from uranium (left) and gold (right) hohlraums. Contour levels are of the (spectral brightness)^3 to cover the wide range of spectral brightness.

This Maximum Credible Yield Memo applies to both uranium and gold hohlraums.

2.3.2 The effects of X-ray Preheat

An x-ray FDS source was extracted from a 2D integrated simulation based on a Au hohlraum and nominal capsule parameters with enforced radiation symmetry. Normally an FDS source is used with multi-group diffusion radiation transport, while the integrated simulation used IMC transport. This difference forces a user to multiply the FDS flux and change its pre-heat content (>1.8 keV) to ensure the FDS simulation matches both the bangtime and yield of the integrated IMC simulation (presumed to be more correct). For this FDS source no overall flux multiplier is needed, but the photon flux above 1.8 keV must be multiplied by 2.2. Rather than use this source in calculations for this memo, we explored the effect of X-ray pre-heat on neutron yield.

High energy X-rays preheat the inner capsule of our imaging double shell and degrade its yield. The 2D integrated yield from the nominal capsule is 2.6e+12 neutrons. The yield from an1D FDS calculation without pre-heat (photons > 1.8 keV) is 2.04e+13, *80 times larger*. Figure 9 shows how the 1D capsule yield degrades as a multiplier is applied to the FDS photons above 1.8 keV. Figure 10 shows that most of the yield degradation is due to photons above 6.0 keV, the gold L-band emission. Because there is uncertainty whether calculations are correct for these high energy X-rays, we have removed all fluxes above 1.8 keV from our FDS source for maximum credible yield estimates.

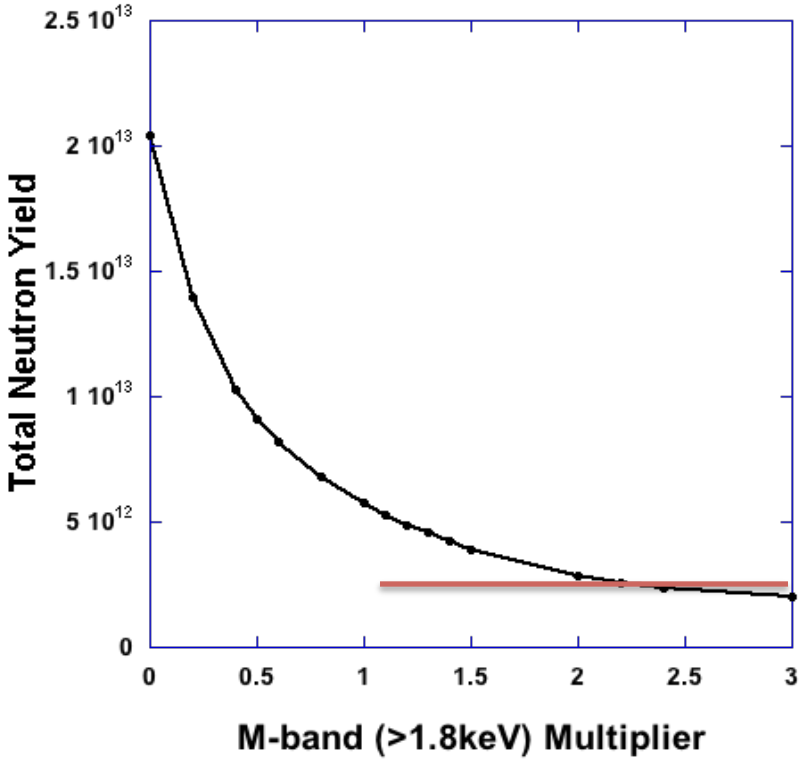

Figure 9. Neutron yield degradation with decreasing pre-heat as a multiplier is applied to photon fluxes above 1.8 keV. The solid red line shows the 2D integrated IMC yield.

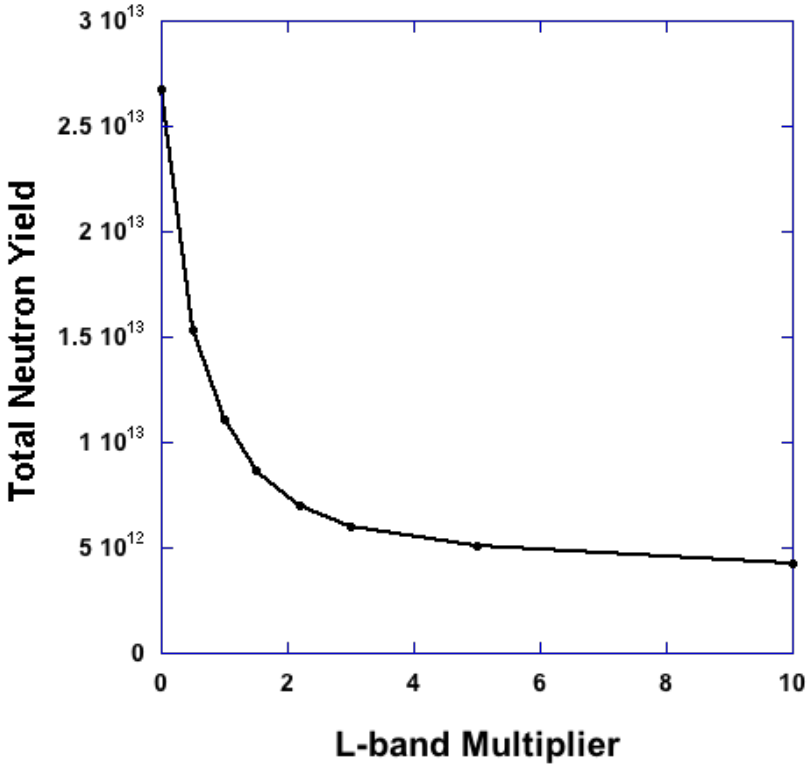

Figure 10. Neutron yield degradation with decreasing pre-heat as a multiplier is applied to photon fluxes above 6.0 keV (L-band).

X-ray preheat degradation has been eliminated from Maximum Credible Yields

2.3.3 Variations in Helium Gas Fill Density

We have explored the affect of hohlraum gas fill density in integrated calculations by varying the fill density from 0.03 to 1.6 mg/cc, i.e. the entire range of gas fills used at NIF. The integrated yield generally increases with gas fill as shown in figure 11. The total X-ray flux , shown in figure 12 , and the hohlraum radiation temperature, shown in figure 13, change little with gas fill density. There is little difference between the M-band (1.8-6.0 keV) emission for different gas fills as shown in figure 14. The effect seems entirely due to less L-band pre-heat. Figure 15 shows how the L-band flux decreases rapidly with hohlraum gas fill density. Figure 10 showed how the neutron yield rose with decreasing L-band flux. A factor of 4 reduction in L-band flux, as changing from 1.6 to 0.1 mg/cc fill density, leads to a factor of 3 increase in 1D yield. The highest credible yield is unchanged by varying hohlraum gas fill from 0.03 to 1.6 mg/cc. In all cases yields are reduce by L-band preheat. But we have already eliminated L- and M-band preheat from our maximum credible yield calculations. For that reason:

The Maximum Credible Yield is not changed by varying hohlraum gas fill from 0.03 to 1.6 mg/cc.

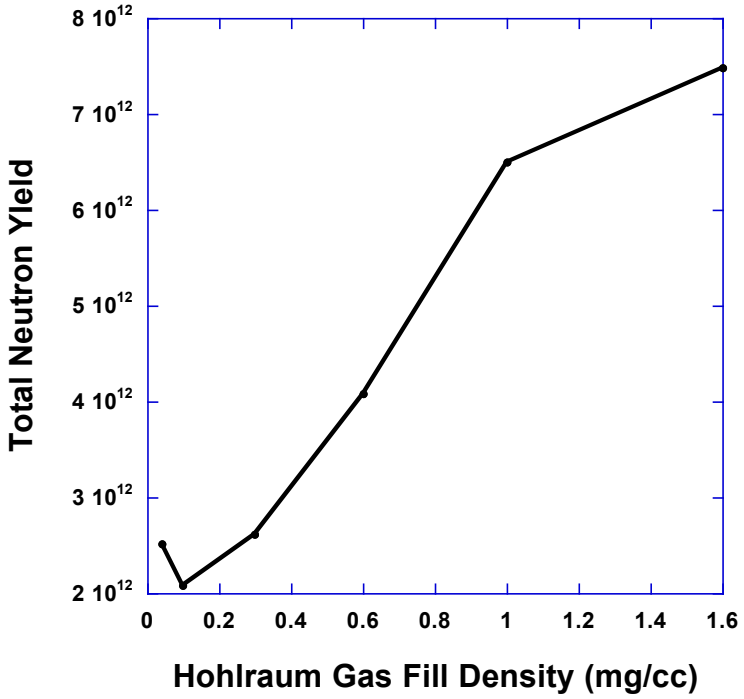

Figure 11. Variation of yield with helium gas fill.

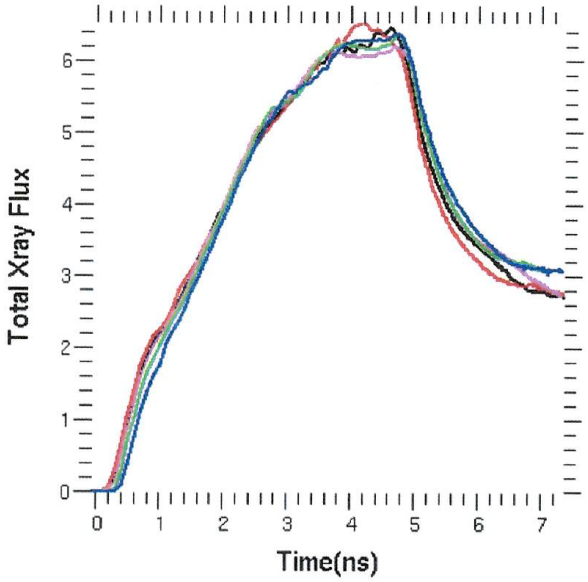

Figure 12. Time dependent variation of total radiation flux for different hohlraum gas fill densities. Black is 0.03 mg/cc;red, 0.1;magenta, 0.6;green, 1.0; and blue, 1.6mg/cc.

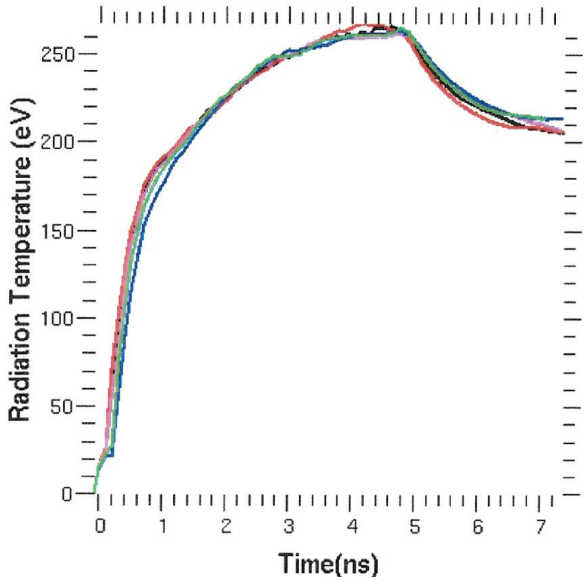

Figure 13. Time dependent variation of hohlraum radiation temperature for different hohlraum gas fill densities. Black is 0.03 mg/cc;red, 0.1;magenta, 0.6;green, 1.0; and blue, 1.6mg/cc.

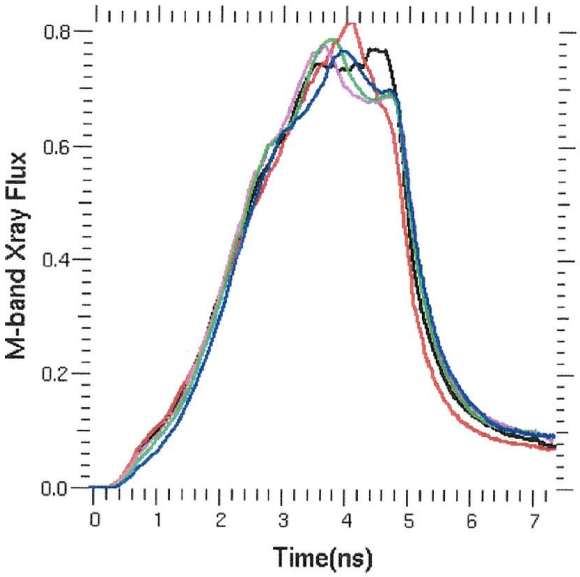

Figure 14. Time dependent variation of M-band (1.8-6.0 keV) radiation flux for different hohlraum gas fill densities. Black is 0.03 mg/cc;red, 0.1;magenta, 0.6;green, 1.0; and blue, 1.6mg/cc.

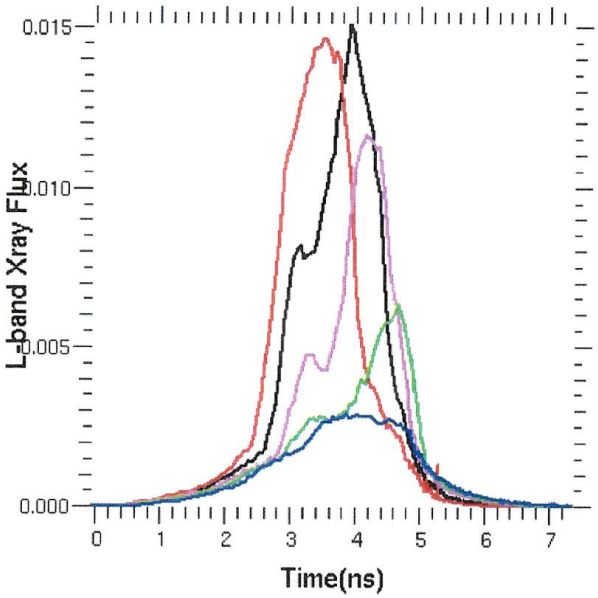

Figure 15. Time dependent variation of L-band (>6.0 keV) radiation flux for different hohlraum gas fill densities. Black is 0.03 mg/cc;red, 0.1;magenta, 0.6;green, 1.0; and blue, 1.6mg/cc.

2.3.4 Variations in Laser Energy, Drive Multiplier, and FDS Flux Multiplier

The total laser energy can be varied in an integrated calculation by multiplying the laser power by a drive multiplier. Our NIF double shell experiments have shown that a value of about 0.88 is needed to replicate experimental implosion times (bangtimes). As used in HYDRA, this is equivalent to using 0.88 times the laser flux at all times and in all beams. To be conservative we have used a 1.0 multiplier in our integrated calculations for maximum credible yields. For 1D simulations we have used a 1.0 multiplier on the FDS fluxes extracted from integrated simulations, which gives the same bangtime as the integrated simulation with the 1.0 drive multiplier. The target total neutron yield as shown in figure 16 peaks at 0.9 to 1.1 MJ in integrated calculations at 2.63 e+12 and falls off at both higher and lower energies. To explore the effects of extra radiation flux in a 1D simulation we have applied a flux multiplier on the FDS source, with the results shown in figure 17. Again the yield peaks at 0.9MJ, then falls off at higher and lower flux. One might assume that at greater flux or higher laser energy the drive X-rays would penetrate more deeply into the aluminum. Then the thickness of the aluminum shell would need to increase to achieve the optimal yield. Section 2.4.1 shows that the optimum yield does NOT increase with laser energy, even when the aluminum thickness is allowed to increase.

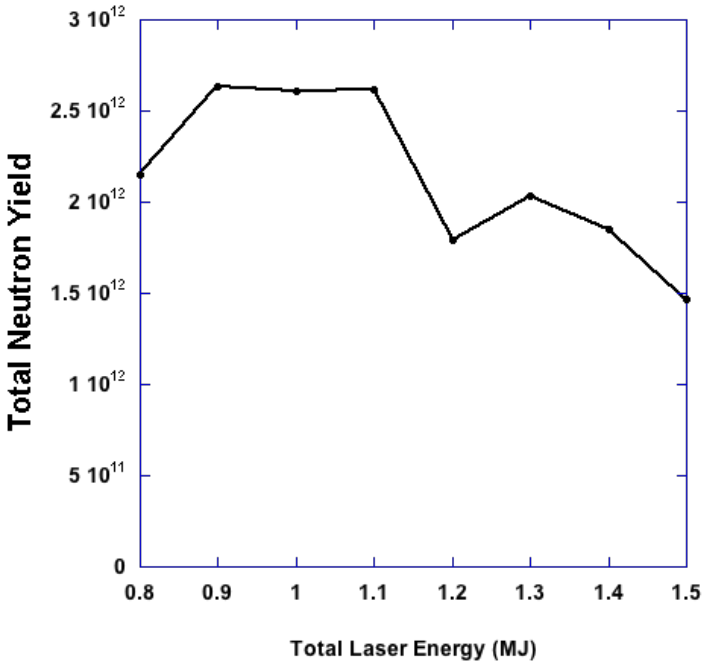

Figure 16. Variation of neutron yield with laser energy, using a power multiplier, in integrated calculations.

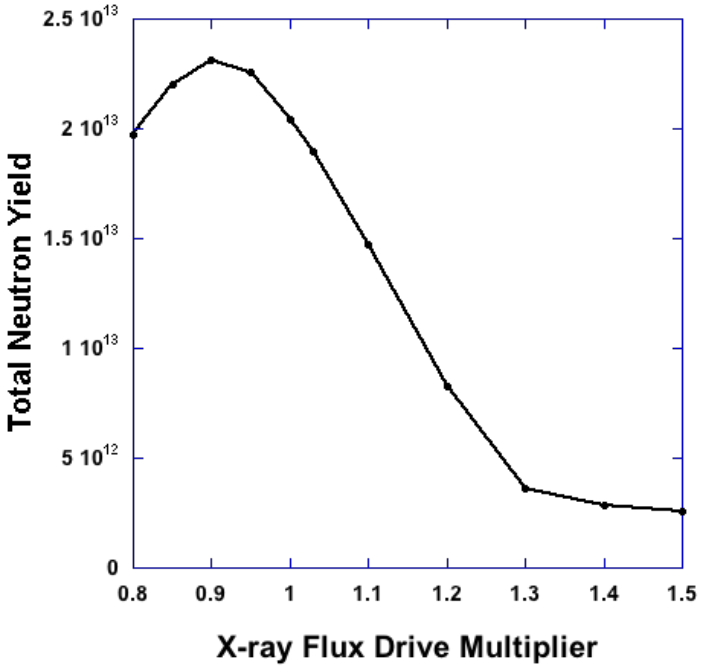

Figure 17. Variation of neutron yield with X-ray fluence in 1D FDS calculations, using a time independent X-ray flux multiplier.

The Maximum Credible Yield occurs at 0.9 MJ or 0.9 FDS flux multiplier.

2.4 Variations in the aluminum ablator

2.4.1 Aluminum Thickness

We expected the optimum yield from a capsule to depend upon aluminum thickness, and that optimum thickness to depend upon the laser energy, or drive multiplier.

Section 2.3.4 discussed how neutron yield varied with laser energy or x-ray flux at the nominal 106 um aluminum shell thickness. Figure 18 shows how the neutron yield varies as both the aluminum thickness and the X-ray flux multiplier are changed. The optimum yield does require an increase in aluminum thickness, from 95 um at a 0.9 multiplier to 140 um at a 1.5 multiplier (1.5 MJ). However, the optimum yield reaches a peak at the 0.9 multiplier. Likewise in integrated calculations at a 1.0 multiplier the yield peaks at 106 um thickness.

Adding dopants with Z higher than 14 (aluminum) will not affect our conclusions. Higher Z dopant in the aluminum will result in less efficient ablation resulting in less inward kinetic energy, giving less yield.

The Maximum Credible Yield is reached at a 0.9 multiplier and 104 um thickness.

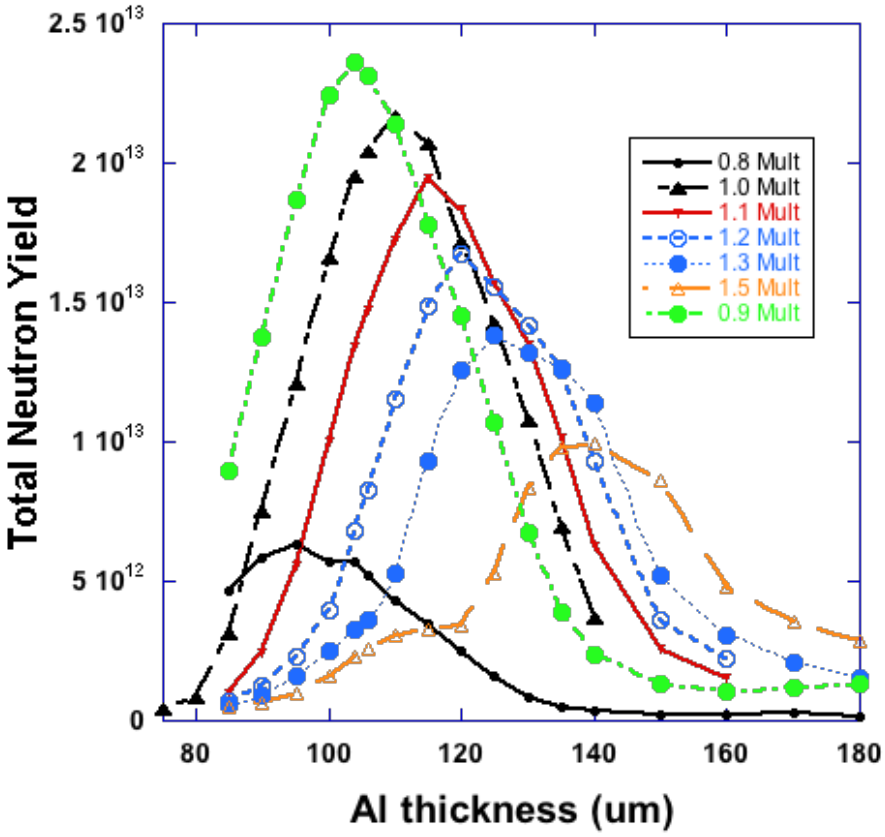

Figure 18. Neutron yield vs laser energy and aluminum shell thickness.

2.4.2 Radius

The outer radius of the aluminum ablator also has a value of 1070 um for optimum yield of 2.6e+13 as shown in figure 18. Smaller radii will absorb less hohlraum energy. The fall off at larger radii seems be due to enhanced radiation penetration at larger radii. Figure 19 shows that the optimum thickness of ablator increases with aluminum shell radius. In these simulations we have used the optimal CH cushion density of 0.015g/cc from section 2.5 rather than the nominal 0.035. The result is higher yields than nominal, which we can use in estimating the maximum credible yield.

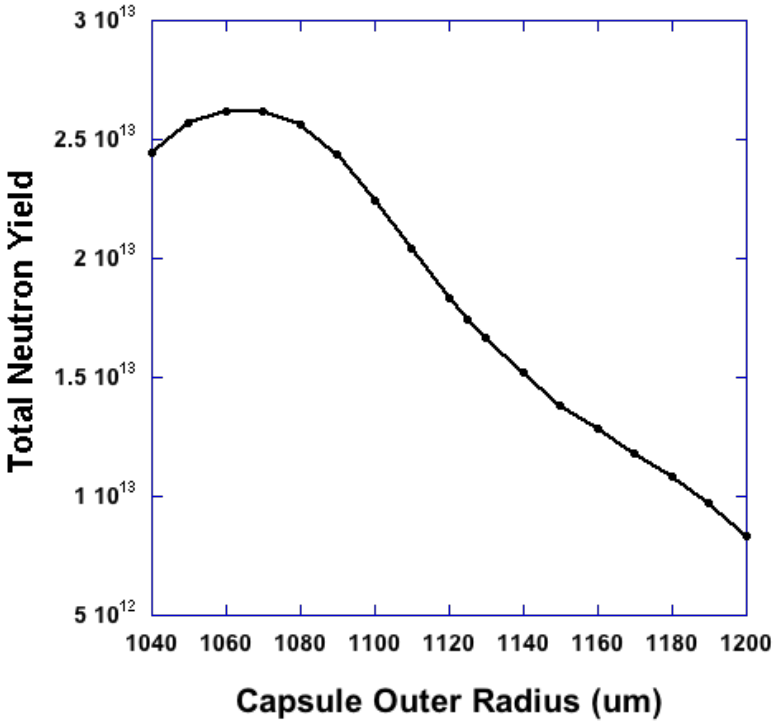

Figure 18. 1D FDS yield as capsule outer radius is varied, with constant 106 um aluminum shell thickness and other parameters nominal.

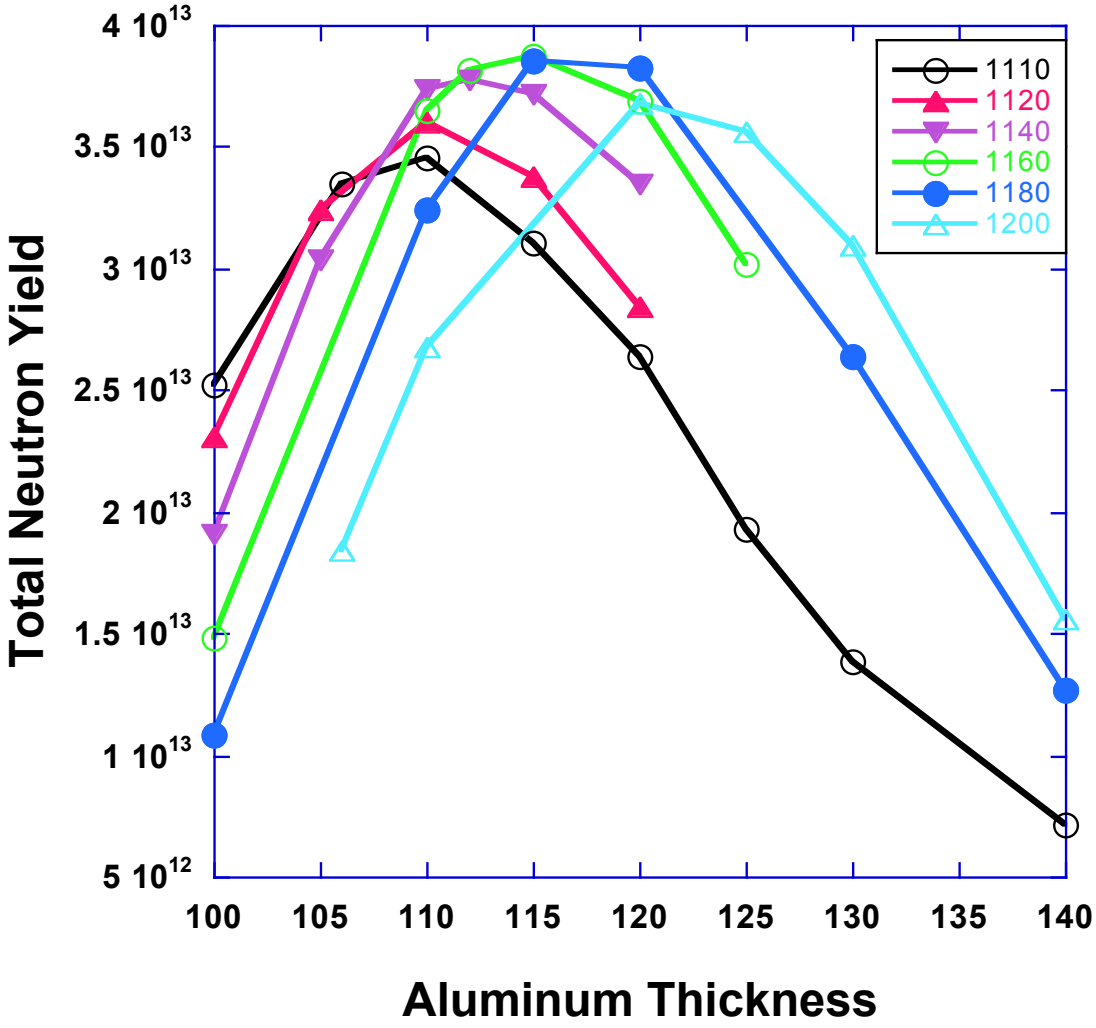

Figure 19. 1D FDS yield with outer radius and aluminum shell thickness varying.

When aluminum thickness is allowed to vary with radius, there is an optimum yield of 3.9e+13 which varies weakly with outer shell radius. This yield, using the optimum cushion density of 0.015 g/cc, will be used in our maximum credible yield estimate. The maximum yield is attained at 115 um aluminum thickness and 1160 um outer radius.

2.5 CH Cushion Foam Density

We have used a CH (polystyrene) cushion between the aluminum outer shell and the inner capsule. Its nominal density is 35 mg/cc. A lower density would give a more efficient implosion, leaving less internal energy remaining in the cushion during and after shell collision. As shown in figure 20 the yield increases down to 15 mg/cc (3.4e+13), then decreases. However only higher densities can be expected to be fabricated and fielded. Since the yield is limited to 3.4e+13, this max cred memo will

allow any density of CH foam to be used. But we will use this optimum foam density in our maximum credible yield estimates.

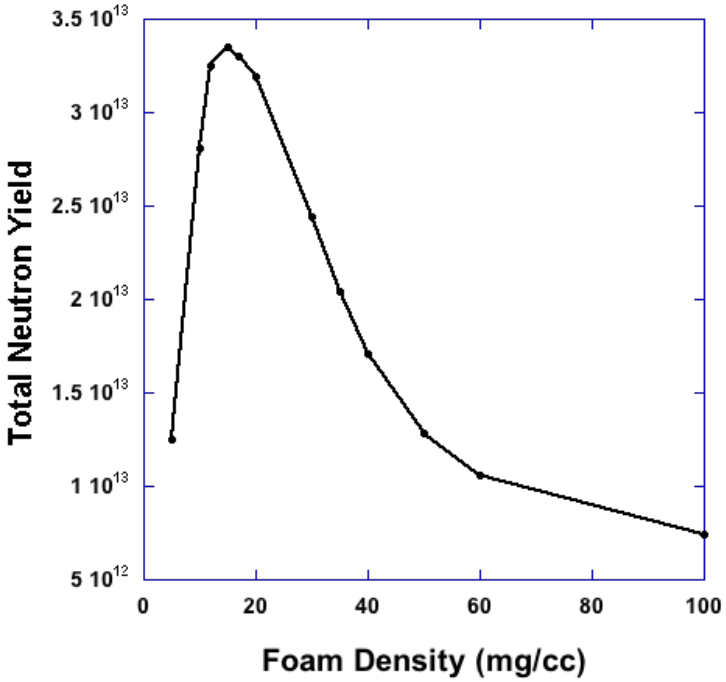

Figure 20. FDS neutron yield at varying CH foam densities with other parameters nominal.

2.6 Inner Shell(s)

Neutron yield is dominated by the density of the deuterium fuel and the inner shell mass. The inner shell mass is affected by the thickness of the GDP layer (equivalently its density) , by the radius of the glass shell, and its thickness. Figures 21, 22, and 23 show how for a fixed GDP and glass density the yield depends upon these parameters. Neutron yield peaks at 20 um GDP thickness, 390 um glass shell outer radius, and 45 um glass thickness. We have used these in determining the maximum credible yield.

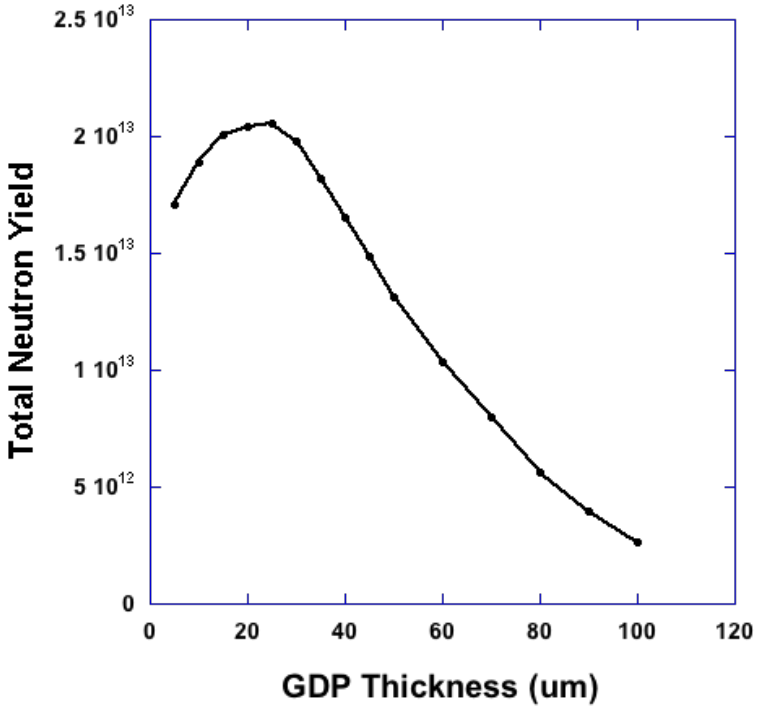

Figure 21. Yield variation with GDP coating thickness in 1D FDS driven calculations.

The Maximum Credible yield applies to any thickness of GDP over-coating the glass shell, including NONE.

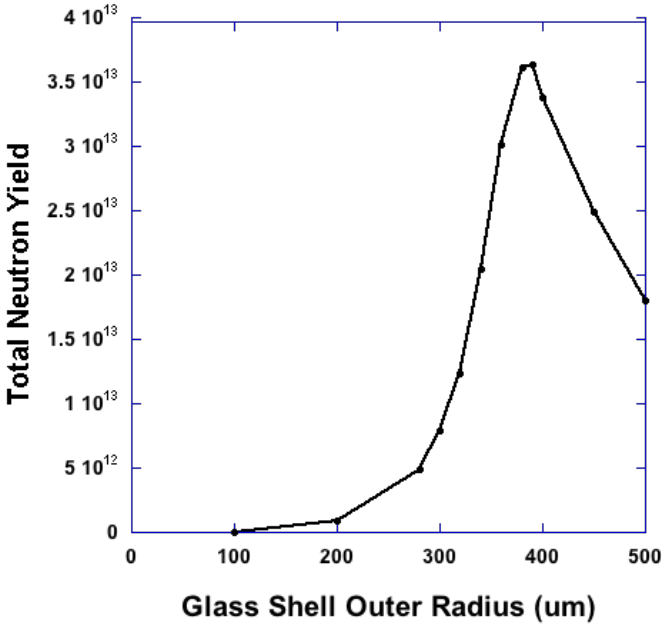

Figure 22. Variation of yield with glass shell outer radius in 1D FDS driven calculations. The peak value is 3.6e+13 neutron at 390 microns thickness.

The Maximum credible yield applies to any glass shell outer radius.

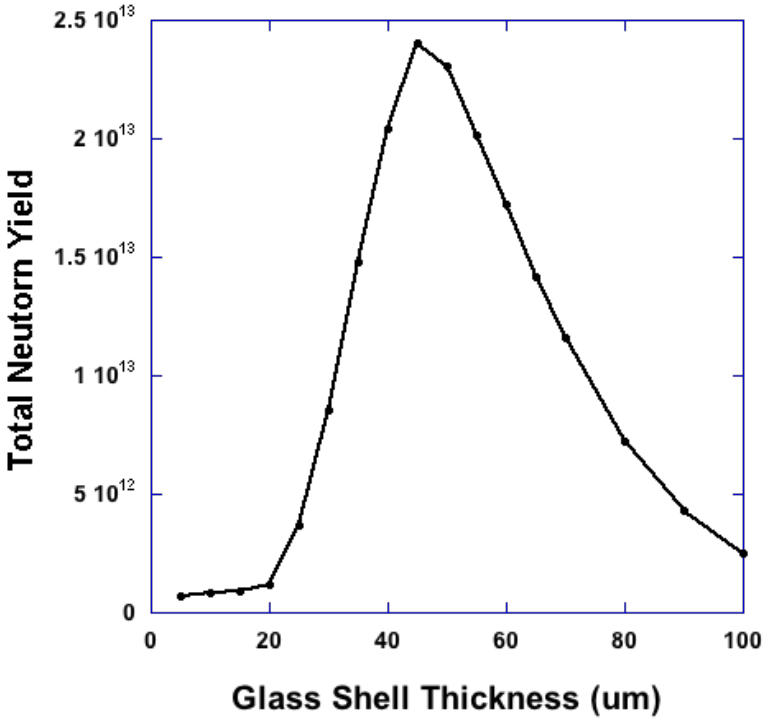

Figure 23. Variation of neutron yield with glass shell thickness in 1D FDS driven calculations. Peak is at 45 um thickness, slightly thicker than nominal. In integrated calculations the peak is at the nominal 40 um thickness.

The Maximum credible yield applies to any glass shell thickness.

2.7 Fuel

This memo addresses pure deuterium and dilutants other than tritium, such as proteum (^{1}H), ^{3}He, and ^{4}He. These dilutants only serve to reduce the fraction of deuterium in the fuel, and the neutron yield. The maximum neutron yield will be produced with 100% deuterium. Figure 24 shows how the yield of 1D FDS (solid) and 2D integrated simulations (triangles) varies as the density of pure deuterium is changed. We have limited the calculations to densities less than liquid deuterium, 16.7 mg/cc, but you can see that the optimal yield occurs at densities of ~ 35 mg/cc. At densities above and below this value the neutron yield decreases. The maximum 1D FDS yield is 2.33e+13, whereas the yield under nominal conditions is 2.04e+13. This maximum yield is less than the maximum credible yield that is derived with combinations of fielding parameters, including deuterium density discussed in section 3.

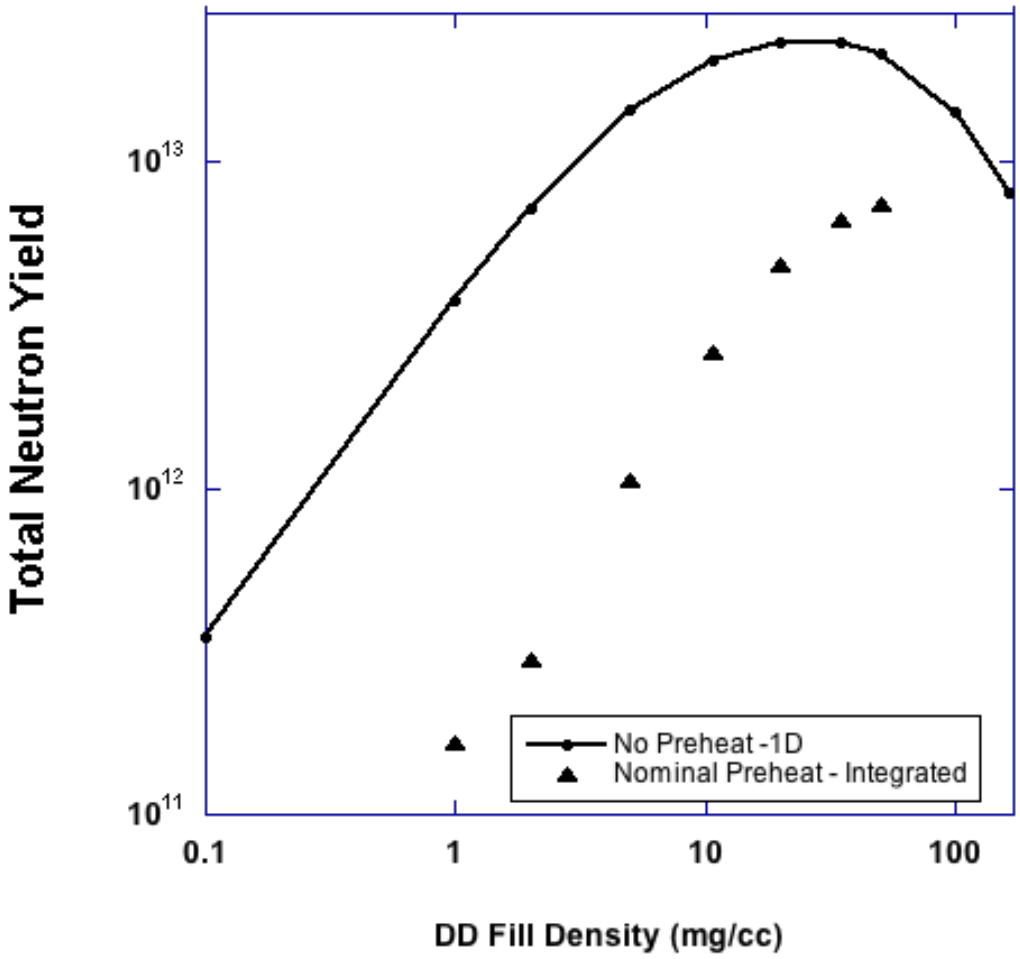

Figure 24. Variation of neutron yield with deuterium fill gas density. Solid are 1D FDS calculations with no preheat, triangles are from 2D integrated symmetric implosions with nominal preheat.

3.0 Maximum credible yield

The maximum credible yield would be the maximum yield obtained with combinations of the parameters. It is not possible to do all combinations of all parameters. Instead we have calculated the yield under a number of optimum conditions. We have studied the maximum yield when a single parameter is varied. The maximum yield in that case is 3.6e+13. When we varied the aluminum radius and thickness together using the optimal cushion density of 0.015 g/cc to get a maximum yield of 3.9e+13. If we use the optimal glass shell radius of 390 um we get 4.39e+13. Allowing the DD density reach its optimum at 20mg/cc and 4.93e+13. Changing the pulse shape from nominal to the 5.87ns fwhm only decreases the yield to 4.07e+13.

Table 2 summarizes those parameter variations from both integrated and 1D FDS driven simulations. We have used the nominal (4.4ns) laser pulse and set all the other parameters in the right column to their optimum values. The yield was 2.77e+13. If instead we used the 5.87ns laser pulse, the yield is 2.34e+13.

We have considered 1D FDS calculations combining optimal parameters in an attempt to find the highest yield in this parameter space. In particular using the individual parameters that gave the highest yields as shown in Table 1, produces a yield of 2.77e+13 neutrons This is higher than any integrated calculation, and greater than most studies varying a single parameter using otherwise nominal parameters. This includes variations of preheat, X-ray drive flux, Aluminum outer radius, aluminum thickness, glass thickness, GDP thickness, and DD density. 2.77e+13 is less the optimum of two single parameter variations, CH foam density (peak 3.4e+13) and glass shell outer radius (3.6e+13). Using the optimum foam density of 0.15mg/cc in 1D FDS simulation, and varying the glass shell outer radius.

Table 2. Summary of Parameter Variations

Parameter	Nominal	Acceptable Range	Highest Yield (Integrated)	Highest Yield (FDS)
Preheat (>1.8keV)	1.0	Any	Not Varied	0.
Laser Energy	1.0 MJ	0-1.5	1.0	0.9
Pulse Length	4.4ns	Any	5.87	5.87
Hohlraum Fill	0.3 mg/cc	0-1.6	1.6	Not relevant
DD Density	10.4 mg/cc	Any	20	35
Glass Shell Radius	340 um	Any	390	390
Glass Thickness	40 um	Any	40	45
GDP Thickness	20	Any	20	25
CH Foam Density	35 mg/cc	Any	20	15
Al Thickness	106 um	Any using 0.8 to 1.5MJ	106	115
Al Outer Radius	1110	0-1200 um	1100	1160
Maximum Yield	2.61e+12	< 1e+14	4.5e+12	4.93e+13

In summary the maximum credible yield under the conditions of table 2 is 5e+13. Most of the uncertainty is in the effects of L-band preheat. It is not credible that the neutron yield would exceed 1e+14.